ELectronics EXpress

Effects of the permittivity and conductivity of human body for normal-mode helical antenna performance

Rasyidah Hanan Mohd Baharin[1a)], Toru Uno[1], Takuji Arima[1], Norsiha Zainuddin[2], Yoshihide Yamada[3], Kamilia Kamardin[3], and Naobumi Michishita[4]

Abstract In the capsule endoscope application, a coil type antenna namely a normal-mode helical antenna was used because of suitable shape to deploy in a cylindrical capsule. In antenna design, many human tissue conditions such as a stomach, fat and skin should be taken into account. Here, losses of human tissues are changed depending on personal differences and basic feature of the antenna in numerical simulation. At some tissue examples, antenna input resistance (R_{in}) increases by the permittivity (ε_r) and conductivity (σ) effect were shown. In order to establish antenna design method, physical mechanism of antenna input resistance increases should be clarified. In this paper, input resistance increases are numerically clarified for all changing conditions of permittivity and conductivity through electromagnetic simulations. As for an antenna, self-resonant normal-mode helical antenna of 0.2 wavelength is designed at 402 MHz. In the case of $\varepsilon_r = 11.6$, the R_{in} value of 0.63 Ω at $\sigma = 0$ [S/m] is increased to the maximum value of $R_{in} = 35\,\Omega$ at $\sigma = 0.3$ [S/m]. For understanding input resistance increases mechanism, electric field distributions around antenna are also shown. To ensure simulation adequateness, a measured result of input resistance is compared with simulated result.
Keywords: normal mode helical antenna, human body
Classification: Devices, circuits and hardware for IoT and biomedical applications

1. Introduction

The interest in research of wireless body area network (WBAN) is demanding and constantly growing. Fig. 1 presents the application of wireless biotelemetry in healthcare system, in which sensor network operating autonomously while connecting the human body to various medical devices.

One example of such device is wireless capsule endoscopy (WCE), in which the antenna is ingested to detect anomaly inside the intestinal tract. Since the introduction of modernized WCE in the year 2000 by Iddan *et al.* [1], many WCE were made commercially available by presti-
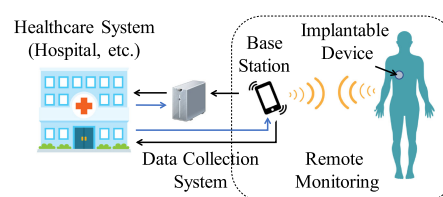
[1]Dept. of Electronic and Information Engineering, Tokyo University of Agriculture and Technology, Koganei, Tokyo 184–8588, Japan
[2]Dept. of Electrical Engineering, Faculty of Engineering, University of Malaya, Kuala Lumpur 50603, Malaysia
[3]Malaysia-Japan International Inst. of Tech., Universiti Teknologi Malaysia, Kuala Lumpur 54100, Malaysia
[4]Dept. of Electrical and Electronic Engineering, National Defense Academy, Yokosuka, Kanagawa 239–8686, Japan
a) rh.baharin@gmail.com

Fig. 1. Wireless biotelemetry in healthcare system.

gious companies, with constant effort in increasing its diagnostic capabilities. This includes PillCam SB (Given Imaging Ltd.), EndoCapsule (Olympus Medical System Corp.), OMOM (Jinshan Science & Technology), MiroCam (Intromedic), Norika-Sayaka (RF Systems Lab), and CapsoCam SV1 (CapsoVision) [2, 3, 4, 5]. Fig. 2(a) shows the generalized cross-section of a WCE unit, which typically contains various sensors, batteries, a transmitter, and an antenna, while 2(b) shows the internal configuration of PillCamSB [6].

(a) General components
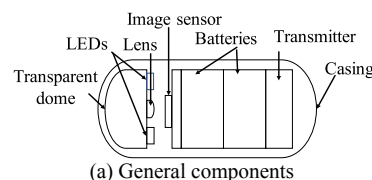
(b) Internal configuration of PillCam SB

Fig. 2. Cross section of WCE [6].

An antenna plays a crucial role in WCE systems. However, designing the in-body antenna to operate at minimum power consumption and making it small is a challenging task [7]. Moreover, there are several requirements to fulfill for the antenna to be effective as a capsule antenna, including: miniaturization to achieve impedance matching at target frequency; spherical electric field distributions that enables transmission anywhere regardless of location of capsule or receiver; diverse polarization that allows efficient transmission regardless of capsule orientation; and straightforward tuning adjustment to compensate human body effect [8, 9]. These can be achieved using helix antenna.

1

Prior studies proposed a few types of antenna to install in WCE including conformal [10, 11, 12, 13], copper-cylinder [14], micro-strip [15], spiral [16, 17], and loop antenna [18]. However, a helix-type antenna is a promising option, as supported by studies that proposes helical-type antenna for a WCE system [19, 20, 21, 22]. Moreover, a helix antenna is a magnetic type antenna, making it more suitable to install inside a non-magnetic body such as the human body tissue. The existing commercial WCE, PillCam SB is installed with internal helix antenna as shown in the previous Fig. 2(b), supports this statement.

Previously, it was suggested that a normal-mode helical antenna (NMHA) is a promising antenna to install inside WCE when the structure is designed at self-resonance, achieving relatively high efficiency at compact size, in free space [23, 24]. As for NMHA embedded in human body, an equation for self-resonant structure was clarified [25]. Some example data for input resistance increase and radiation field decrease were shown [26, 27, 28]. However, to date, systematic understanding regarding the phenomena of input resistance (R_{in}) and radiation changes of NMHA corresponding to permittivity and conductivity was not clarified. To contribute to the design of capsule endoscope using this antenna, there is a need to investigate the changes from lossless to lossy by varying the conductivity.

It is noted that the actual σ of fat, skin, and stomach at 402 MHz are given as $\sigma = 0.08$, 0.69, and 1.0 [S/m], respectively [29, 30]. Furthermore, the real conductivity of tissues can never be lossless. However, individual differences are relatively large in actual human bodies where both the relative permittivity and conductivity changes in some interval. Hence, the relative permittivity and conductivity is treated independently particularly for this study.

In this paper, input resistance and radiation field changes by both changes of permittivity and conductivity are numerically clarified. Effects of permittivity and conductivity for electric characteristic changes are systematically shown. Moreover, by fabricating a human body phantom, measured results of electrical characteristics are obtained.

2. Fundamental equations of NMHA

2.1 Equivalent electric current model
The equivalent electrical current model is shown in Fig. 3. The feed is set at the center of the antenna. The input impedance (Z_{in}) of NMHA can be expressed by Eq. (1), consisting of input resistance (R_{in}), and complex reactances (jX). Meanwhile, R_{in} consists of small dipole resistance
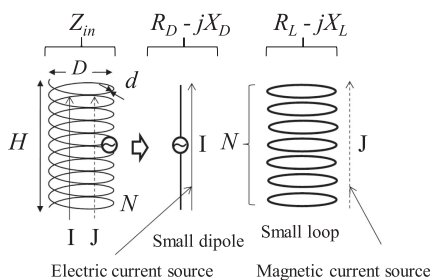
(R_D), small loop resistance (R_L), and ohmic resistance of wire (R_o) shown in Eq. (2). The summation of R_D and R_L is equal to the antenna resistance, denoted by R_a (Eq. (3)). The conditions that allows this assumption will be explained in section 3. Meanwhile, the reactances X, consisting of capacitive reactance (X_D) and inductive reactance (X_L) are sourced from small dipole and small loop, respectively as shown in Eq. (4).

$$Z_{in} = R_{in} + jX \tag{1}$$

$$R_{in} = R_D + R_L + R_o \tag{2}$$

$$R_a = R_D + R_L \tag{3}$$

$$X = X_L - X_D \tag{4}$$

2.2 Self-resonant equation
Self-resonance of NMHA is achieved when the reactance component is equivalent and cancel out each other ($X_L = X_D$), resulting in Z_{in} becoming pure resistance, R_{in}. Prior study has established the self-resonant equation in human body condition [25]. The equation relates the parameters of NMHA (N, D, H) to human body related parameters (ε_r, λ_g) as shown in Eq. (5). Here, ε_r and λ_g indicates the permittivity and wavelength in a human body, respectively.

$$\sqrt{\frac{1}{\varepsilon_r}} \frac{600\pi \times 19.7N\left(\dfrac{D}{\lambda_g}\right)^2}{9\left(\dfrac{D}{\lambda_g}\right) + 20\left(\dfrac{H}{\lambda_g}\right)} = \sqrt{\varepsilon_r} \frac{125\left(\dfrac{H}{\lambda_g}\right)}{\pi N\left(1.1\dfrac{H}{\lambda_g} + \dfrac{D}{\lambda_g}\right)^2} \tag{5}$$

The left and right-side terms correspond to X_L and X_D, respectively. Due to the structural variables (H, D) are normalized by wavelength, the structural equation is very universal.

3. Simulation results

3.1 Simulation parameters
Simulation model is set as following; NMHA at selected parameter is embedded inside the center of homogenous cylindrical phantom as shown in Fig. 4, assumed as a solid-shaped dielectric body. The antenna is put in a small capsule and a small air gap is placed between the antenna and phantom.
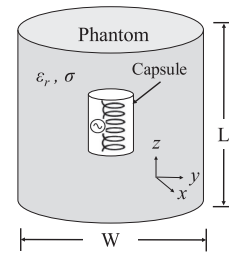

Fig. 4. NMHA embedded inside phantom model.

The simulation parameters are summarized in Table I. Simulation was performed using a Method of Moment (MoM) method, using FEKO 7.0 software. Even though the original motive of the study is centered on WCE


Fig. 3. Equivalent electric current model of NMHA.

2

Table I. Simulation parameters.

Parameter	Item/Values
Simulation	FEKO with Method of Moment (MoM)
Frequency	402 MHz (MICS)
Dielectric phantom	Permittivity, ε_r = 70.6 (stomach); 46.7 (skin); 11.6 (fat) Conductivity, σ = 0; 0.3; 1.1 [S/m] Mesh size of phantom, $\Delta p = \lambda_g/30$ L = W = 30 mm
Antenna wire	Material = copper; Diameter of wire, d = 1.2 mm; Conductivity, $\sigma_w = 58 \times 10^6$ [1/Ωm] (copper); No. of turns, N = 5; 7; 9 Mesh size of antenna wire, $\Delta w = \lambda_g/100$

application, ε_r at different tissues that possibly surrounds the stomach, namely skin and fat were also studied.

3.2 Self-resonant structure

Self-resonant structure of NMHA can be obtained by solving Eq. (5). As for simulations, resonance is achieved by adjusting parameters H and D for a given N, at selected frequency 402 MHz. Self-resonant structures are shown in Fig. 5. D and H is normalized to the wavelength of the human body, λ_g.

The self-resonant curves obtained by Eq. (5) and simulation agree with each other and allow us to ensure antenna parameters (D, H) used in the simulation are correct. It is interesting that the structures are not affected by σ. Six points labelled A to F are chosen to investigate the effect of ε_r and σ with respect to R_{in}.
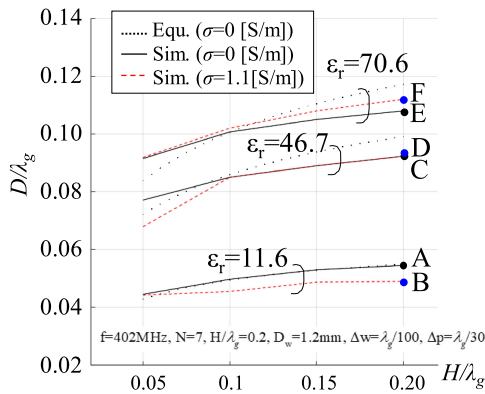
Fig. 5. Self-resonant structure of NMHA in human body.

3.3 Input resistance when ε_r and σ varied

At self-resonant structures, antenna input impedance becomes pure resistance (R_{in}). In the previous study, it was reported that input resistance was increased as a result of σ increase. In Fig. 6, input impedance characteristics at the structure E and F are shown. Black circle points indicate self-resonant points at 402 MHz. The apparent resistance shift of NMHA is observed. The resistance increases 19 Ω from E to F.

To see the trends more clearly, Fig. 7 is plotted, elaborating data of R_{in} at more discrete points of σ.

At σ = 0 [S/m], R_{in} of structures A, C, and E become $R_{in}(A) = 0.63 \, \Omega$, $R_{in}(C) = 0.31 \, \Omega$, and $R_{in}(E) = 1.37 \, \Omega$,
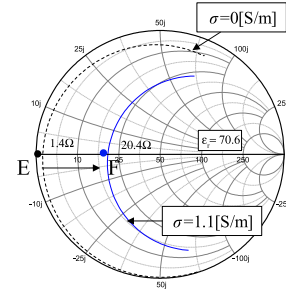
Fig. 6. Input impedance in smith chart for structures E and F.
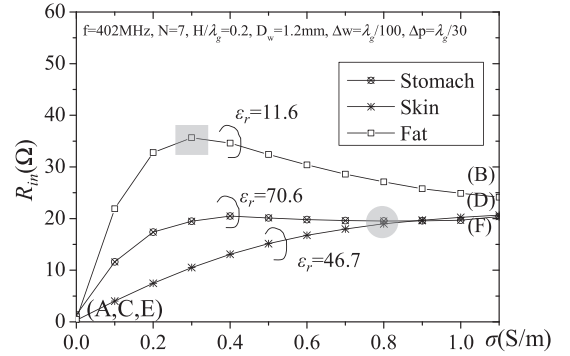
Fig. 7. Input impedance across tissues of different permittivity and conductivity.

respectively. One intriguing finding from the Fig. 7 is in lower permittivity tissue, fat (ε_r = 11.6), where NMHA exhibits the steepest R_{in} increase compared to the other two with its highest magnitude at σ = 0.3 [S/m], ($R_{in} = 35 \, \Omega$), as noted in the square-shaped region. As for stomach and skin, the R_{in} experiences steady rise, then stays constant from σ = 0.8 [S/m] and higher, shown by the circle-shaped region. As a summary of R_{in} dependence on ε_r, it's clear that R_{in} increases in accordance with the increase of σ. As for R_{in} dependence on ε_r, it is strange that the curves of ε_r = 70.6 exists between curves of ε_r = 46.7 and ε_r = 11.6. For ε_r dependence, study of more data such as electric field distributions are needed.

3.4 Near field distribution

In order to realize R_{in} dependencies on ε_r and σ, near field distributions of electric fields are calculated. In Fig. 8, 9, and 10, electric field distributions are shown for ε_r = 11.6, ε_r = 46.7, and ε_r = 70.6, respectively. As for σ changes, significant points of Fig. 7 such as σ = 0, 0.3, and 1.1 [S/m] are selected.

The magnitude of maximum value of received power is denoted by $|S_{21}|$. S_{21} power may relate to the produced power at the antenna that is expressed by $P_a = V^2/R_{in}$. S_{21} will be inversely proportional to R_{in}. At σ = 0.3 [S/m], S_{21} are observed as 78, 95, and 97 dBV for ε_r values of 11.6, 70.6, and 46.6, respectively. This ε_r order corresponds to the ε_r order shown in Fig. 7. At σ = 1.1 [S/m], S_{21} values become the same for ε_r of 11.6, 70.6, and 46.6, respectively as shown in Fig. 7.

The near field distribution discussed in Fig. 8 to 10 is important as the standard procedure of SAR estimation can be done based on electric field data [31, 32]. Based on SAR
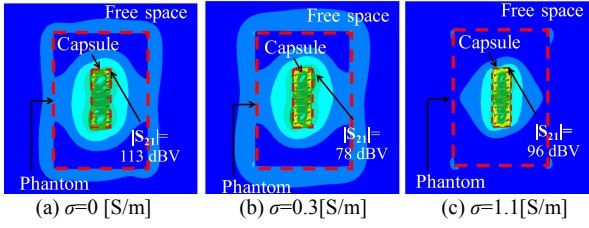
3

Fig. 8. Distribution of electric field for dielectric with permittivity, $\varepsilon_r = 11.6$ (presumably fat tissue).
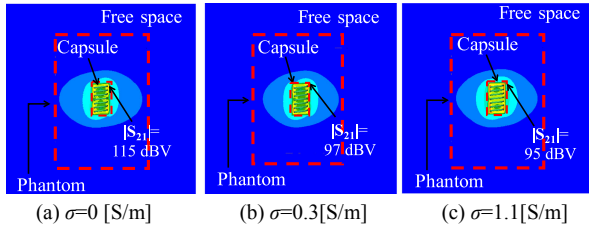

Fig. 9. Distribution of electric field for dielectric with permittivity, $\varepsilon_r = 46.7$ (presumably skin tissue).
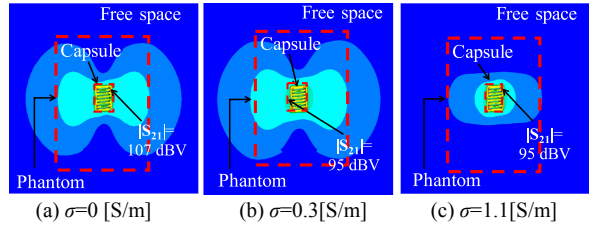

Fig. 10. Distribution of electric field for dielectric with permittivity, $\varepsilon_r = 70.6$ (presumably stomach tissue).

formula relating electric field to conductivity, one would expect that the increasing conductivities will result on decrease of electrical field. However, the SAR values may also be influenced by impedance matching, which is influenced by dielectric properties [33]. Since early in this paper it was clarified that the NMHA is tuned to resonance, this explains the inconsistent trends of S_{21} from Fig. 8 to 10.
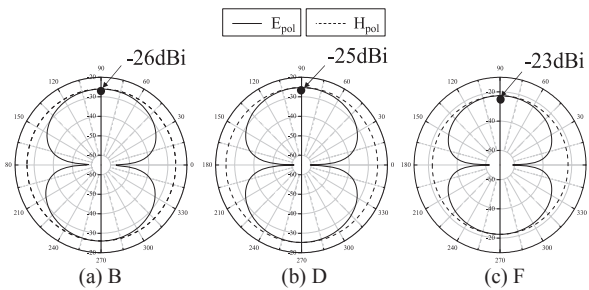
3.5 Radiation pattern

Fig. 11. Radiation patterns.

The far-field contains important information to roughly estimate the angular properties of the radiated field. Calculated radiation patterns at structures B, D, and F are shown in Fig. 11. The solid line is E-polarization while dotted lines show H-polarization. Antenna gains, (G_A) become -26 dBi, -25 dBi and -23 dBi at structures B, D, and F,

respectively. In order to understand small antenna gains, input resistance values are shown in Table II. For obtaining R_a value that correspond to radiation resistance, antenna wire conductivity (σ_w) is set very large such as $\sigma_w = 10^{10}$ [S/m] [34]. Then, the antenna efficiency (η_a) is calculated by the next equation.

$$\eta_a = \frac{R_a}{R_{in}(\sigma = 1.1)} \qquad (6)$$

Meanwhile, η_a values are also shown in Table II.

Table II. Calculation of efficiency, η_{pha}.

Parameters		$\sigma = 0$ [S/m]		$\sigma = 1.1$ [S/m]		
Struct.	ε_r	R_a [Ω]	$R_{in(\sigma=0)}$ [Ω]	Struct.	$R_{in(\sigma=1.1)}$ [Ω]	η_a
A	11.6	0.307	0.485	B	24.1	-18.9 dB
C	46.7	0.155	0.307	D	20.7	-21.5 dB
E	70.6	1.222	1.370	F	20.4	-12.2 dB

From Table II, η_a for structure B and D is approaching the same values as that of Fig. 11, while F shows largest difference of -11 dB from that of Fig. 11(c). In order to estimate antenna gain, some factors such as impedance mismatch between the material and free space, and radio wave propagation loss in a material must be considered. However, η_a degradation by an increase of R_{in} plays an important part for determining G_A value.

4. Fabrication and measurement
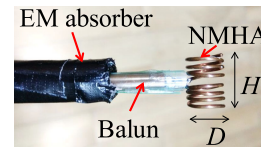
4.1 Fabrication of antenna and phantom

Fig. 12. Fabricated NMHA.

First, NMHA is fabricated at one selected point (F) as shown in Fig. 12. The balun acts as suppressor of reverse current. A stomach phantom was fabricated depending on the list of ingredients shown in Table III. In the table, the role of respective ingredients is also briefly highlighted [35, 36]. The dielectric constants, ε_r and σ were measured at 8 points on the fabricated phantom.

Table III. Recipe of phantom and their attributes

Material	Weight (g)	Role
Distilled water	400	Main ingredient
Polyethylene powder	6	Permittivity
Agar	17.5	Shaping and curing agent
Sodium chloride	1.925	Conductivity
Xanthan gum	15	Adhesive agent
Sodium dehydro-acetate	0.25	Preservative

The averaged value of measured dielectric constant is $\varepsilon_r = 70.6$ and $\sigma = 1.1$ [S/m]. So, this dielectric constant is selected in the previous sections.

4.2 Measured results

Measurement result of input impedance is shown in Fig. 13. At point F, the impedance is $21.1\,\Omega$ (measured) and $20.4\,\Omega$ (simulation). As for radiation pattern, comparing to the dipole antenna level, antenna gain (G_A) is obtained as shown in Fig. 14. By the next equation;

$$G_A = 2.15\,\text{dBi} - (51\,\text{dBm} - 25\,\text{dBm})\,[\text{dBi}] \qquad (7)$$

G_A becomes -23.85 dBi. This value agrees well with the calculated value of -23 dBi of Fig. 11(c). Good agreement between simulated and measured results ensure correctness of the simulation model.

5. Conclusion

Antenna input resistance dependence on permittivity and conductivity is systematically clarified. From the electromagnetic results, it is shown that input resistance is monotonously increased in accordance with the increase of conductivity. However, dependence on permittivity is has no direct correlation especially in the low permittivity tissues, such as fat. By electric field distribution, it is hypothesized that how the near field is dispersed in the surface of phantom have a major effect on impedance of antenna. A simple method for estimation of antenna efficiency, gain, and loss factor is also proposed. Measured results of selected points agree well with the simulation, ensuring the correctness of the simulation model.
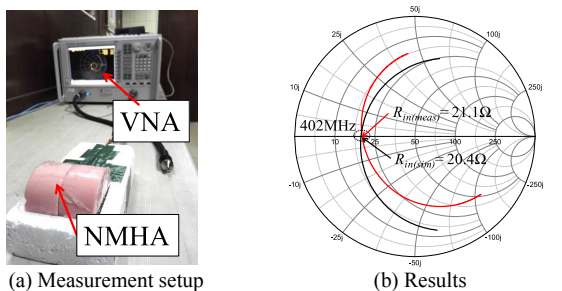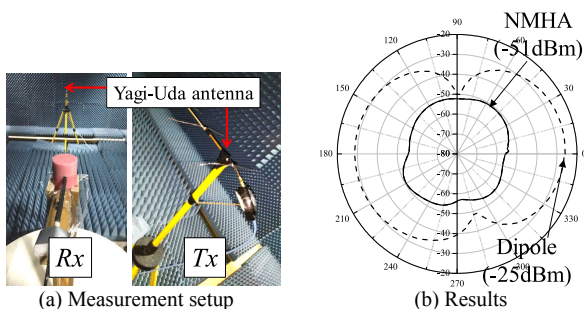

Fig. 13. Input impedance measurement.

Fig. 14. Radiation pattern measurement.

References

[1] G. Iddan, et al.: "Wireless capsule endoscopy," Nature **405** (2000) 417 (DOI: 10.1038/35013140).

[2] E. Rondonotti, et al.: "Small-bowel capsule endoscopy and device-assisted enteroscopy for diagnosis and treatment of small-bowel disorders: European society of gastrointestinal endoscopy (ESGE) technical review," Endoscopy **50** (2018) 423 (DOI: 10.1055/a-0576-0566).

[3] M. R. Basar, et al.: "Ingestible wireless capsule technology: A review of development and future indication," Int. J. Antennas Propag. **2012** (2012) 807165 (DOI: 10.1155/2012/807165).

[4] R. Scott and R. Enns: "Advances in capsule endoscopy," Gastroenterol. Hepatol. **11** (2015) 612.

[5] A. Wang, et al.: "Wireless capsule endoscopy," Gastrointest. Endosc. **78** (2013) 805 (DOI: 10.1016/j.gie.2013.06.026).

[6] N. Kurniawan and M. Keuchel: in *Video Capsule Endoscopy: A Reference Guide and Atlas*, ed. M. Keuchel, et al. (Springer, Berlin, Germany, 2014) 15–20.

[7] M. Norris, et al.: "Sub miniature antenna design for wireless implants," Proc. of the IET Seminar on Antennas and Propagation for Body-Centric Wireless Communication 2007 (2007) (DOI: 10.1049/ic:20070547).

[8] Z. Wang, et al.: "Review of the wireless capsule transmitting and receiving antennas," in *Wireless Communications and Networks - Recent Advances*, ed. A. Eksim (InTech, 2012) ISBN: 978-953-51-0189-5.

[9] K. S. Nikita: "Antennas and RF communication," *Handbook of Biomedical Telemetry* (Wiley-IEEE Press, 2014) 1.

[10] J. Wang, et al.: "An implantable and conformal antenna for wireless capsule endoscopy," IEEE Antennas Wireless Propag. Lett. **17** (2018) 1153 (DOI: 10.1109/LAWP.2018.2836392).

[11] R. Alrawashdeh, et al.: "A new small conformal antenna for capsule endoscopy," 2013 7th European Conference on Antennas and Propagation (EuCAP) (2013) 220.

[12] J. Faerber, et al.: "Design of conformal wideband antennas for capsule endoscopy within a body tissue environment," 2016 46th European Microwave Conference (EuMC) (2016) 1223 (DOI: 10.1109/EuMC.2016.7824570).

[13] J. Faerber, et al.: "In vivo characterization of a wireless telemetry module for a capsule endoscopy system utilizing a conformal antenna," IEEE Trans. Biomed. Circuits Syst. **12** (2018) 95 (DOI: 10.1109/TBCAS.2017.2759254).

[14] Z. Duan, et al.: "Integrated design of wideband omnidirectional antenna and electronic components for wireless capsule endoscopy systems," IEEE Access **6** (2018) 29626 (DOI: 10.1109/ACCESS.2018.2840689).

[15] M. Kaffa, et al.: "Design of microstrip antenna for wireless capsule endoscopy in wireless body area network," 2017 IEEE Asia Pacific Conference on Wireless and Mobile (APWiMob) (2017) 134 (DOI: 10.1109/APWiMob.2017.8283996).

[16] A. P. George and M. Sujatha: "Imbedded spiral antenna for endoscope," International Conference on Information Communication and Embedded Systems (ICICES2014) (2014) 1 (DOI: 10.1109/ICICES.2014.7034105).

[17] S. H. Lee, *et al.*: "A wideband spiral antenna for ingestible capsule endoscope systems: Experimental results in a human phantom and a pig," IEEE Trans. Biomed. Eng. **58** (2011) 1734 (DOI: 10.1109/TBME.2011.2112659).

[18] R. S. Alrawashdeh, *et al.*: "A broadband flexible implantable loop antenna with complementary split ring resonators," IEEE Antennas Wireless Propag. Lett. **14** (2015) 1506 (DOI: 10.1109/LAWP.2015.2403952).

[19] M. Takahashi: "Antennas for wireless power transmission of capsule endoscope," 2018 IEEE International Workshop on Electromagnetics: Applications and Student Innovation Competition (iWEM) (2018) 1 (DOI: 10.1109/iWEM.2018.8536724).

[20] S. I. Kwak, *et al.*: "The helical antenna for the capsule endoscope," 2005 IEEE Antennas and Propagation Society International Symposium **2B** (2005) 804 (DOI: 10.1109/APS.2005.1552139).

[21] Y. Morimoto, *et al.*: "Design of ultra wide-band low-band implant antennas for capsule endoscope application," 2013 7th International Symposium on Medical Information and Communication Technology (ISMICT) (2013) 61 (DOI: 10.1109/ISMICT.2013.6521700).

[22] C. Liu, *et al.*: "Circularly polarized helical antenna for ISM-band ingestible capsule endoscope systems," IEEE Trans. Antennas Propag. **62** (2014) 6027 (DOI: 10.1109/TAP.2014.2364074).

[23] Q. D. Nguyen, *et al.*: "Deterministic equation for self-resonant structures of very small normal-mode helical antennas," IEICE Trans. Commun. **E94-B** (2011) 1276 (DOI: 10.1587/transcom.E94.B.1276).

[24] D. T. Dung, *et al.*: "Investigating equations used to design a very small normal-mode helical antenna in free space," Int. J. Antennas Propag. **2018** (2018) 7967468 (DOI: 10.1155/2018/7967468).

[25] N. T. Tuan: "Development of small normal-mode helical antenna used for human body sensors," M. Phil Dissertation, Universiti Teknologi Malaysia, Kuala Lumpur (2017).

[26] N. T. Tuan, *et al.*: "Simulation accuracy of normal-mode helical antenna used in human body," 2016 International Symposium on Antennas and Propagation (ISAP) (2016) 168.

[27] D. T. Dung, *et al.*: "Electric characteristics of very small normal-mode helical antenna in human body conditions," 2017 International Conference on Advanced Technologies for Communications (ATC) (2017) 70 (DOI: 10.1109/ATC.2017.8167645).

[28] N. T. Tuan, *et al.*: "Deterministic equation of self-resonant structures for normal-mode helical antennas implanted in a human body," IEEE Antennas Wireless Propag. Lett. **17** (2018) 1377 (DOI: 10.1109/LAWP.2018.2846600).

[29] Australian Communications Authority (2003): "Planning for medical implant communications systems (MICS) & related devices," Document: SPP 6/03.

[30] J. Kim and Y. Rahmat-Samii: "Implanted antennas inside a human body: Simulations, designs, and characterizations," IEEE Trans. Microw. Theory Techn. **52** (2004) 1934 (DOI: 10.1109/TMTT.2004.832018).

[31] M. Terzi, *et al.*: "The role of electromagnetic fields in neurological disorders," J. Chem. Neuroanat. **75** (2016) 77 (DOI: 10.1016/j.jchemneu.2016.04.003).

[32] S. Lee, *et al.*: "Design of an implanted compact antenna for an artificial cardiac pacemaker system," IEICE Electron. Express **8** (2011) 2112 (DOI: 10.1587/elex.8.2112).

[33] L. Xu, *et al.*: "Effects of dielectric parameters of human body on radiation characteristics of ingestible wireless device at operating frequency of 430 MHz," IEEE Trans. Biomed. Eng. **56** (2009) 2083 (DOI: 10.1109/TBME.2009.2021157).

[34] R. H. B. M. Baharin, *et al.*: "Input resistances of small normal-mode helical antennas in dielectric materials," 2017 IEEE Asia Pacific Microwave Conference (APMC) (2017) 1175 (DOI: 10.1109/APMC.2017.8251667).

[35] T. Yamamoto, *et al.*: "Development of electromagnetic phantom at low-frequency band," 2013 35th Annual International Conference of the IEEE Engineering in Medicine and Biology Society (EMBC) (2013) 1887 (DOI: 10.1109/EMBC.2013.6609893).

[36] K. Ito: "Human body phantoms for evaluation of wearable and implantable antennas," The Second European Conference on Antennas and Propagation, EuCAP 2007 (2007) 1 (DOI: 10.1049/ic.2007.1117).